ELSEVIER

Physica E 3 (1998) 112–120

PHYSICA E

Electronic states in quantum dot atoms and molecules

S. Tarucha [a,*], T. Honda [a], D.G. Austing [a], Y. Tokura [a], K. Muraki [a], T.H. Oosterkamp [b], J.W. Janssen [b], L.P. Kouwenhoven [b]

[a] *NTT Basic Research Laboratories, 3-1, Morinosato Wakamiya, Atsugi-shi, Kanagawa 243-0124, Japan*
[b] *Department of Applied Physics and DIMES, Delft University of Technology, PO Box 5046, 2600 GA Delft, The Netherlands*

Abstract

We study electronic states in disk-shaped semiconductor artificial atoms and molecules containing just a few electrons. The few-electron ground states in the artificial atom show atomic-like properties such as a shell structure and obey Hund's rule. A magnetic field induces transitions in the ground states, which are identified as crossings between single particle states, singlet–triplet transitions and spin polarization. These properties are discussed in conjunction with exact calculation in which the effect of finite thickness of the disk is taken into account. An artificial molecule is made from vertically coupling two disk-shaped dots. When the two dots are quantum mechanically strongly coupled, the few-electron ground states are de-localized throughout the system and the electronic properties resemble those of a single artificial atom.

PACS: 73.20.Dx; 72.20.My; 73.40.Gk

Keywords: Artificial atom; Artificial molecule; Quantum dot; Excitation spectroscopy; Coulomb oscillations

1. Introduction

Semiconductor quantum dots are often referred to as artificial atoms since their electronic properties, for example the ionization energy and discrete excitation spectrum, resemble those of real atoms [1,2]. We have recently fabricated a circular disk-shaped quantum dot, and observed atomic-like properties by measuring Coulomb oscillations [3]. Electrons bound to a nuclear potential experience sufficiently strong quantum mechanical confinement and mutual Coulomb interactions that they are well arranged in ordered states. This leads to the ordering of atoms in the periodic table. The ionization energy has large principal maxima for atomic numbers $2, 10, 18, \ldots$ when certain orbitals are completely filled with electrons. In addition, for the filling of electrons in similar orbitals Hund's rule favours parallel spins until the set of orbitals is half-filled. This also gives rise to secondary maxima in the ionization energy. The disk-shaped quantum dot we can fabricate is formed in a laterally gated double barrier structure, and contains a tunable number of electrons starting from zero. Associated with the rotational symmetry of the lateral confinement, we observe a two-dimensional (2D) "shell structure" from the addi-

* Corresponding author. Tel.: +81 462 40 3445; fax: +81 462 40 4723; e-mail: tarucha@will.brl.ntt.co.jp.

1386-9477/98/$ – see front matter
PII: S1386-9477(98)00225-2

tion energies, analogous to the three-dimensional (3D) shell structure for atomic ionization energies. In addition, spin effects such as a pairing of Coulomb oscillation peaks due to spin degeneracy, and modifications of the pairing in line with Hund's rule are all observed. In real atoms, electrons are so strongly trapped that their quantum mechanical properties are not accessible by means of conventional spectroscopic techniques. In contrast, the electrons in our quantum dot are bound in a relatively large region of the order of 100 nm. This allows us to use readily accessible magnetic fields not only to identify the quantum mechanical states, but also to induce transitions in the ground states which are expected but never tested in real atoms on earth [4]. In this paper, we first discuss the addition energy spectrum of the ground states at zero magnetic field, and magnetic field induced transitions in the ground states for a different number of electrons, N, in a disk-shaped dot. We employ an exact diagonalization technique incorporating many body interactions, and the effect of a finite thickness of the dot disk, to understand the magnetic field induced transitions of ground states. The effect of finite thickness weakens the Coulomb interactions relative to the quantum mechanical confinement. In our previous calculation [4] we neglected this effect, and assumed that the Coulomb interactions were weaker than those reproduced in the experiment. We show here that a good agreement with experiment is now obtained with a realistic interaction model. For the next set after artificial atoms, we outline how vertically coupled disk-shaped dots can be employed to study the filling of electrons in artificial molecules. We show that in a quantum mechanically strongly coupled double dot system the electronic states are delocalized.

2. Device fabrication and experimental set up

Fig. 1a shows a schematic diagram of the device which consists of an n-doped GaAs substrate, with undoped layers of 7.5 nm $Al_{0.22}Ga_{0.78}As$, 12 nm $In_{0.05}Ga_{0.95}As$, and 9.0 nm $Al_{0.22}Ga_{0.78}As$, and $a \approx$ 500 nm n-doped GaAs top layer. A sub-micronmeter pillar (geometrical diameter, D) is fabricated using

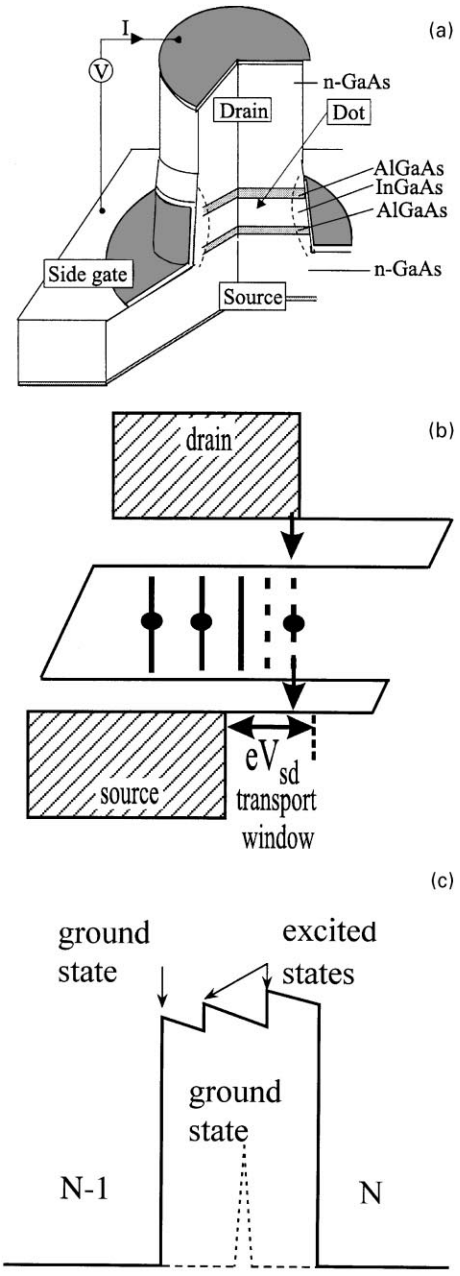

Fig. 1. (a) Schematic diagram of the device containing a disk-shaped dot. (b) Schematic energy (horizontal axis) diagram along the vertical axis of the pillar. Hatched regions are occupied electron states in source and drain contacts. For the case shown, two electrons are permanently trapped in the quantum dot. The third electron can choose to tunnel through the $N = 3$ ground state (solid line) or through one of the two excited states which lie in the transport window. (c) Schematic of tunneling current vs. gate voltage for a sufficiently small V_{sd} (dashed line) that only the ground state contributes to the current, and for a larger V_{sd} (solid line) that allows both the ground and excited states to contribute to the current. For the case of the large V_{sd}, a small jump in the current stripe identifies where an excited state enters the transport window.

electron beam lithography and etching techniques [5]. Source and drain electrical wires are connected to the top and substrate contacts. A third wire is attached to the metal that is wrapped around the pillar. This electrode is the side gate. The energy landscape along the vertical axis is shown in Fig. 1b. The $In_{0.05}Ga_{0.95}As$ layer has a disk shape. By making the gate voltage, V_g, more negative we can electrically squeeze the effective diameter of this disk from a few hundred nanometers down to zero. Application of a bias voltage, V_{sd}, between the source and drain opens a "transport window" between the Fermi energies of the source and drain for detecting both the ground and excited states in the dot (Fig. 1b). Ground and excited states lying within the transport window can contribute to the current. If the gate voltage is made more positive, then the levels in Fig. 1b shift down in energy. When V_{sd} is smaller than the energy difference between the ground and lowest excited state, only the ground state contributes to the current, I, because the electron tunneling into the excited state is blocked by the charging of the ground state. This is the usual case for the measurement of Coulomb oscillations, so we see a series of current "peaks" as a function of gate voltage corresponding to the one-by-one change of electrons in the ground states of the dot (Fig. 1c). When V_{sd} is large enough, however, both ground and excited states can be within the transport window, and contribute to the current. Electron tunneling into the excited states can occur following the electron escape from a ground state. I vs. V_g therefore becomes a series of current "stripes". Small jumps inside the stripe measure when excited states enter the transport window. Each current stripe falls off when the ground state leaves the transport window, so it has a width in energy given by eV_{sd}. We employ this technique to study the excitation spectrum. Our samples are measured while mounted in a dilution refrigerator. Due to pick-up of noise the effective electron temperature is about 100 mK.

3. Electronic states in quantum dot atoms

3.1. Ground state spectroscopy

Fig. 2a shows I vs. V_g for single quantum dot ($D = 0.5\,\mu m$) measured at a small V_{sd} of 0.15 mV so that only the ground states contribute to the current.

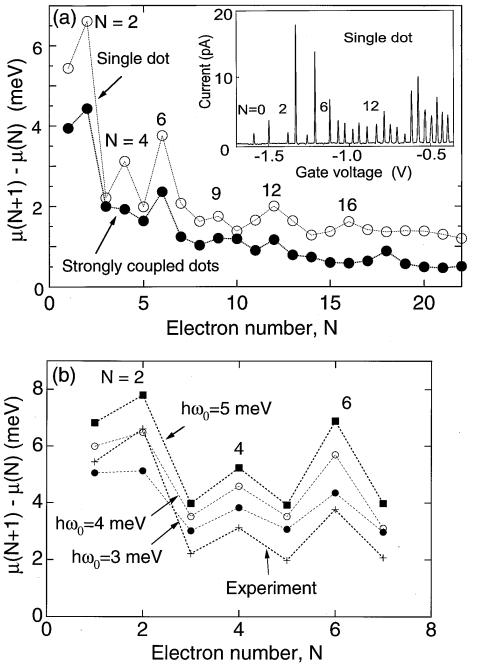

Fig. 2. (a) Change of electrochemical potential vs. electron number for a single dot ($D = 0.5\,\mu m$ open circles) and also for two strongly coupled dots ($D = 0.56\,\mu m$ solid circles; see Section 4 in the text). The inset shows the Coulomb oscillations measured for $V_{sd} = 0.15\,mV$ at $B = 0\,T$ for the single dot. (b) Change of the electrochemical potential calculated for the single dot shown in Fig. 2a. Three different $\hbar\omega_0$ values of 3, 4 and 5 meV are taken as parameters. The experimental data for the single dot in Fig. 2a is also shown by the crosses for comparison.

The current oscillations arise from the one-by-one change of electrons trapped in the dot. The absolute values of N can be identified in each zero-current region (Coulomb blockade region) between the peaks, starting from $N = 0$, because for $V_g < -1.6\,V$ the dot is empty. When N becomes smaller than 20, the oscillation period depends strongly on N. In contrast, Coulomb oscillations observed for a large dot containing more than 100 electrons look very periodic (data not shown; see Ref. [6]), as expected from classical Coulomb blockade theory. The current peak to the left of a Coulomb blockade region with N trapped electrons thus measures the N-electron ground state energy (or electrochemical potential, $\mu(N)$, of the N-electron dot). For example, the first, second and third peaks from the left measure the one, two and three electron ground state energies, respectively. The peak

spacing labeled by "N" therefore corresponds to the energy difference $\mu(N+1)-\mu(N)$ between the N and $N+1$ electron ground states. This energy difference, which can also be determined from measurement of the widths of the so-called "Coulomb diamonds" [2], is plotted as a function of N in Fig. 2a. In correspondence to the spacings between the Coulomb oscillations, the energy difference is unusually large for $N=2$, 6 and 12, and is also relatively large for $N=4$, 9 and 16. The values of 2, 6 and 12 arise from the complete filling of the first, second and third shells, respectively, while those of 4, 9 and 16 are due, respectively, to the half filling of the second, third and fourth shells with parallel spins in accordance with Hund's rule [3]. We compare the data in Fig. 2a with an exact calculation for $N=1$ to 7 shown in Fig. 2b. This calculation incorporates the effect of the finite thickness of the disk. We note that this effect weakens the Coulomb interactions in the dot, and thus makes the shell structure more visible. The thin disk thickness freezes the electrons in the lowest state in the vertical direction. We therefore only have to consider the confinement in the plane of the disk for which we take a parabolic potential $V(r)=\frac{1}{2}m^*\omega_0^2 r^2$, where $m^*=0.06m_0$ is the effective mass of electrons in the InGaAs disk, ω_0 is the characteristic frequency of the lateral confinement and r is the distance measured from the center of the disk. Details of the calculation technique are given in Ref. [7]. The strength of the Coulomb interactions can be represented by a parameter $Q=e^2/\varepsilon l_0$, where l_0 $(=\sqrt{\hbar/m^*\omega_0})$ is the spatial extension of the lowest state's wave function for parabolic confinement. As ω_0 becomes large, or as the quantum mechanical confinement becomes strong, the strength of Coulomb interactions relative to that of quantum confinement $(=Q/\hbar\omega_0)$ becomes progressively small $(\propto \omega_0^{-3/2})$ [8]. Consequently, as $\hbar\omega_0$ varies from 3 to 5 meV in the calculation, the $N=2$ and 6 peaks linked to the complete filling of shells become significantly large as compared to the $N=4$ peak. If we inspect carefully the peaks relative to the background, we find that the agreement with the experimental data is good for $\hbar\omega_0>4$ meV when $N\leqslant 2$, and becomes better for a smaller $\hbar\omega_0$ value as N increases. Note that in the calculation the $N=2$ peak is almost missing for $\hbar\omega_0=3$ meV and the $N=6$ peak is too high for $\hbar\omega_0=5$ meV to reproduce the experiment. These arguments on $\hbar\omega_0$ are also supported by the experiment

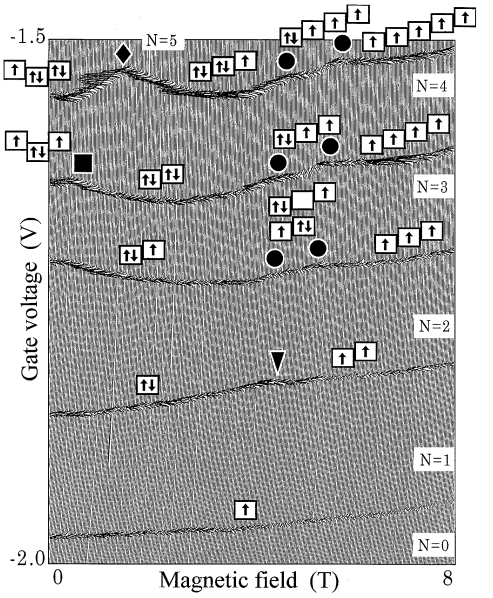

Fig. 3. $I(V_g,B)$ for $N=0$ to 5 measured with small $V_{sd}=0.1$ mV such that only ground states contribute to the current. Different types of ground state transitions are indicated by different labels. The arrows in the squares indicate the spin configuration. The lowest square corresponds to a single particle state with angular momentum $l=0$. For squares to the right l increases to 1, 2, 3, etc. For $N=4$ and 5, near $B=0$ T, also the $l=-1$ square is shown to the left of the $l=0$ square.

on the B-field dependence of the Coulomb oscillation peaks (see Ref. [3] and Section 3.3). Decrease of $\hbar\omega_0$ with increasing N can be explained by the effect of Coulomb screening from the leads and gates which is not incorporated in the calculation [9]. We note that the background relative to the peaks is significantly smaller in the calculation than that in the experiment. This can also be due to the screening effect.

Fig. 3 shows the magnetic field dependence of the first five current peaks for $V_{sd}=0.1$ mV. The single dot device is similar to, but not the same as, that used for the experiment of Fig. 2a. The B-field dependence of the peak positions in gate voltage reflects the evolution of the ground state energies. Besides an overall smooth B-field dependence, we see several kinks, which we indicate by different labels. As we discuss in the following section, these kinks are assigned to transitions in the ground states, so for the regions between the kinks, we can identify the quantum numbers, including the spin configurations.

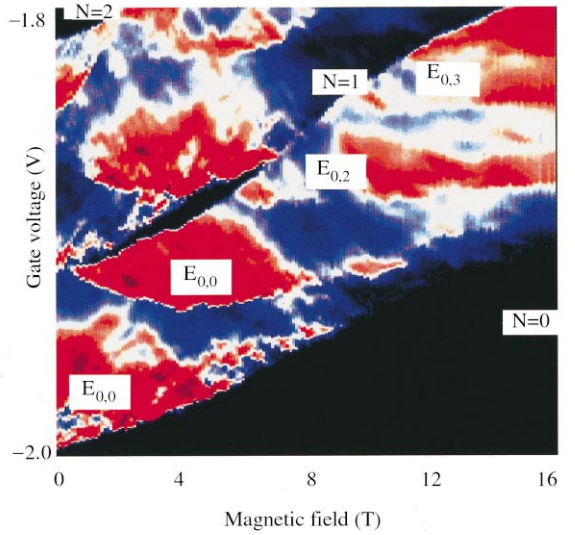

Fig. 4. $I(V_g, B)$ for $N = 0$ to 2 measured with $V_{sd} = 5$ mV up to 16 T. $I < 0.1$ pA in the dark blue regions and $I > 10$ pA in the dark red regions. Both the ground state and the first few excited states can contribute to the current. Current stripes between the Coulomb blockade regions (black) for $N = 0$ and 1 electrons, and for $N = 1$ and 2 electrons are the first and second current stripes, respectively. The states in the first stripe are indexed by the quantum numbers (n, l).

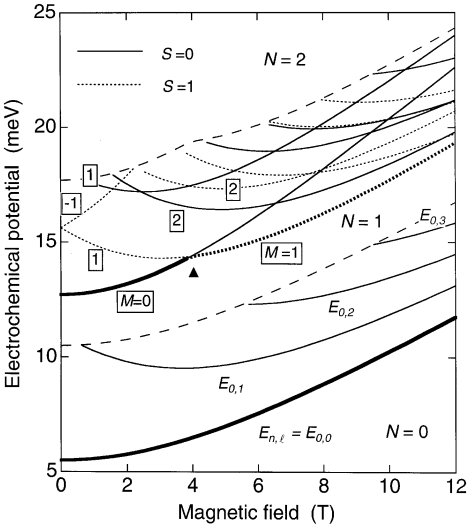

Fig. 5. Exact calculations of the ground states (thick lines) and excited states (thin lines) for $N = 1$ and 2. The $N = 1$ states are indexed by single-particle eigenenergies $E_{n,l}$. The $N = 2$ many-body states are indexed by the total spin and total angular momentum (boxed number). The lowest thick line of each stripe is the ground state energy. The upper thin dashed line of each stripe is the ground state energy shifted upwards by 5 meV. The solid and dotted lines indicate $S = 0$ and 1 configurations, respectively. The label ▲ is discussed in the text.

3.2. Excitation spectroscopy

To investigate what kind of many-body states are responsible for the kinks observed in Fig. 3, we measure I vs. V_g for a large V_{sd} of 5 mV. The data are shown in Fig. 4 for $N = 1$ and 2. For this particular voltage, the two stripes just touch at $B = 0$ T. A pronounced current change, as indicated by the colour change from dark blue to red (i.e. from < 1 pA to > 10 pA), enters the upper edge of the first stripe at $B = 0.2$ T. This change identifies the position of the first excited state for the $N = 1$ dot (we discuss the index $E_{0,1}$ below). Note that at higher B values two higher excited states also enter from the upper edge of the stripe at 5.7 and 9.5 T, respectively. The energy separation between the ground state and the first excited state can be read directly from the relative position inside the stripe. So, the excitation energy ($= \hbar\omega_0$) is slightly larger than 5 meV at $B = 0$ T and decreases for increasing B. Note that even over this wide magnetic field range of 16 T, the first excited state never crosses with the ground state (lower edge of the stripe). In the second stripe of Fig. 4, however, we see the first excited state cross with the ground state at $B = 4.15$ T, i.e. the first excited state for $B < 4.15$ T (seen as the current change from blue to red inside the second stripe) becomes the ground state for $B > 4.15$ T. Located exactly at this magnetic field is the kink labeled by ▼ in Fig. 3, so it is assigned to a crossing between the ground state and the first excited state. In a similar fashion, we are able to identify a crossing between the ground state and the first excited state corresponding to each kink in Fig. 3 [4].

3.3. Exact calculation of many-body states

For a few electrons the energy spectrum can be calculated exactly [10]. Fig. 5 shows exact calculations of the electrochemical potential vs. B for the $N = 1$ and 2 ground states (thick lines) and excited states (thin lines). We use $\hbar\omega_0$ of 5.5 meV and make the same assumptions as those taken above in Section 3.1. For

each stripe the lower thick line is the ground state, and the upper thin dashed line is the lower thick line shifted upwards by 5 meV. This indicates the transport window for $V_{sd} = 5$ mV. For the first electron the exact calculation gives single particle states. The eigenenergies with radial quantum number $n = 0, 1, 2, \ldots$ and angular momentum quantum number $l = 0, \pm 1, \pm 2, \ldots$ are given by [11]

$$E_{n,l} = (2n + |l| + 1)h\sqrt{\left(\tfrac{1}{4}\omega_c^2 + \omega_0^2\right)} - \tfrac{1}{2}lh\omega_c, \qquad (1)$$

where the cyclotron frequency $\omega_c = eB/m^*$. (We neglect the much smaller Zeeman energy.) The states lying within this transport window can be compared with the observed current changes seen in the first stripe of Fig. 4. The agreement is very good for both the ground state and the first excited state over the whole B-field range. For the $N = 2$ case, many excited states are lying within the transport window. We index the ground and excited states by the total spin, S, and the total angular momentum, M (boxed number). The solid and dotted lines indicate the $S = 0$ (spin singlet) and $S = 1$ (spin triplet) states, respectively. Whilst the $N = 1$ ground state $E_{0,0}$ never crosses with the first excited state, we see a crossing (labeled by ▲) between the ground state with $(S, M) = (0, 0)$ and the excited state with $(S, M) = (1, 0)$, which is referred to as singlet–triplet transition [12]. For $\hbar\omega_0 = 5.5$ meV this singlet–triplet transition is expected at $B = 4.0$ T, which is in good agreement with the experimental value in Figs. 3 and 4. Note that the calculated excited states with $(S, M) = (1, -1)$ and $(0, 2)$ for $N = 2$ can also be seen in the second stripe of Fig. 4 (i.e. the lines between blue and red current regions which show a maximum near ~2 T). The $(1, -1)$ is located ≈3 meV above the ground state of $(0, 0)$ at $B = 0$ T. This position is well predicted by the calculation of Fig. 5. The excitation energy is significantly smaller than the single-particle excitation energy of $E_{0,1}$ $(= \hbar\omega_0)$ due to the exchange effect of the parallel spin of the electrons for the $(S, M) = (1, -1)$ state.

Now we discuss the energy spectrum for $N = 3$ and 4. Exact calculations of the ground and excited states are shown in Fig. 6. The three electron ground state has two transitions labeled by ●. On increasing B, the total spin and the total angular momentum of the many-body states change from $(S, M) = (1/2, 1)$ to $(1/2, 2)$ at 4.3 T, and then to $(3/2, 3)$ at 4.8 T. The transitions to

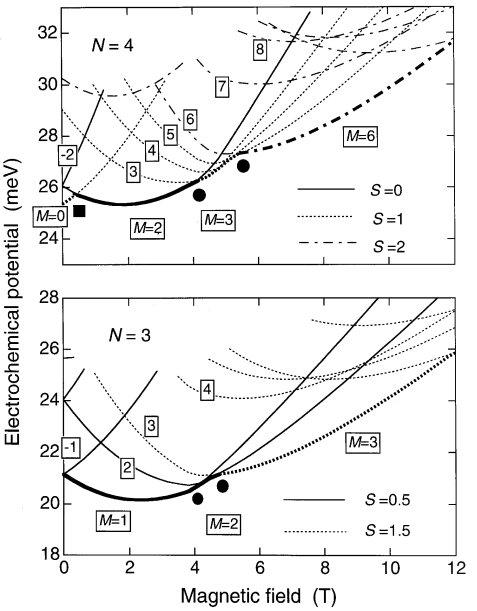

Fig. 6. Exact calculations of ground states (thick lines) and excited states (thin lines) for $N = 3$ and 4. Many-body states are indexed by the total spin and angular momentum (boxed numbers). For $N = 3$, the solid and dotted lines indicate $S = 0.5$ and 1.5, respectively. For $N = 4$, the solid, dotted and dot-dashed lines indicate $S = 0$, 1 and 2 respectively. The ■, ● labels are discussed in the text.

larger angular momentum states reduce the Coulomb interactions. In addition, the total spin increases to gain exchange energy. A double transition in the ground state energy is indeed observed in the form of two kinks in the third peak trace of Fig. 3. In most regions in Fig. 3 there is one main configuration for the occupation of single-particle states. For $N = 3$, however, in the region between the two ● labels there are two important configurations, which both have the same total spin, and total angular momentum. The four electron ground state has five transitions: $(S, M) = (1, 0)$ to $(0, 2)$ at 0.43 T, then to $(1, 3)$ at 4.0 T, to $(1, 4)$ at 4.9 T, to $(1, 5)$ at 5.2 T, and finally to $(2, 6)$ at 5.4 T, respectively. The first transition (labeled by ■) is associated with breakdown of Hund's rule [3] and the other transitions can be understood in the same way as discussed above for the three electron ground state. These transitions are indeed observed as kinks in Fig. 3. The transitions between the two ● labels are not so evident in the experimental data. This is prob-

ably because different states in this region lie close in energy, and the ground state does not show a critical change in electrochemical potential at the transition points (see Fig. 6). We note that the first few excited states in the calculation of Fig. 6 are also observed in the measurement of the excitation spectra [4]. For B larger than the right most ● for $N = 3$ and 4 there is again a distinct ground state in which the electrons are fully spin-polarized and occupy sequential momentum states.

4. Electronic states in quantum dot molecules

A quantum dot molecule can be realized in the same vertical device configuration as for a quantum dot atom except that the double barrier structure is replaced by a triple barrier structure [13]. The outer barriers have the same thickness of 7.0 nm. Quantum mechanical coupling between the two dots form symmetric and anti-symmetric states. By changing the thickness of the central barrier, b, from 7.5 to 2.5 nm we are able to increase the energy splitting between symmetric and anti-symmetric states, $\Delta_{\mathrm{S\,AS}}$, from about 0.09 to 3.4 meV. Quantum mechanically, we consider the dots separated by a 7.5 nm barrier to be "weakly" coupled, and the dots separated by a 2.5 nm barrier to be "strongly" coupled. As a rough guide, for the case of two electrons trapped in the system ($N = 2$), the lateral confinement energy, $\hbar\omega_0$, $= 4$ meV, a typical average "classical" charging energy, $E_{\mathrm{classical}} = 3$ meV, and an electrostatic coupling energy, $E_{\mathrm{electrostatic}} = 0.7$ meV respectively are comparable to $\Delta_{\mathrm{S\,AS}}$ for $b = 2.4, 2.8$, and 4.8 nm. The $\hbar\omega_0$ value is slightly smaller than that for a single dot probably because the lateral electrostatic confinement is weaker as the system is larger. We note that quantum mechanical coupling is not the only coupling mechanism in *artificial molecules*. In the regime where ($\hbar\omega_0 >$) $E_{\mathrm{electrostatic}} \gg \Delta_{\mathrm{S\,AS}}$, it is electrostatic coupling between the dots which becomes important [14]. Competition between the two mechanisms as b is varied is expected to have a profound effect on the transport properties of the two dot system. Here we focus on the strongly coupled double dot system.

Fig. 7 shows a grey scale plot of $\mathrm{d}I/\mathrm{d}V_{\mathrm{sd}}$ in the V_{sd}–V_{g} plane for a $D = 0.56\,\mu$m "strongly" coupled double dot device ($b = 2.5$ nm). Black (positive values of $\mathrm{d}I/\mathrm{d}V_{\mathrm{sd}}$) and white (negative values of $\mathrm{d}I/\mathrm{d}V_{\mathrm{sd}}$) lines criss-crossing the plot and running parallel to the sides of the diamonds identify bound and excited states – details of which will be published elsewhere. Well formed Coulomb diamonds (grey regions where $I = 0$ pA) close to zero bias from $N = 1$ to 22 are evident. The symmetry of the diamonds with respect to the bias direction confirms that the states responsible are indeed delocalized over both dots. Notice that the $N = 2$, and $N = 6$ diamonds are unusually large compared to the adjoining diamonds. As for the single dot the half width of the Nth diamond is a direct measure of $\mu(N + 1) - \mu(N)$. The $\mu(N + 1) - \mu(N)$ values obtained from Fig. 7 are shown by the black circles in Fig. 2b. For this double dot device we see the same magic numbers 2, 6, and 12 as for the single dot device although, intriguingly, and for reasons which are not yet understood, 4, 9, and 16 are apparently absent. The 3 meV value of $E_{\mathrm{classical}}$ is also in

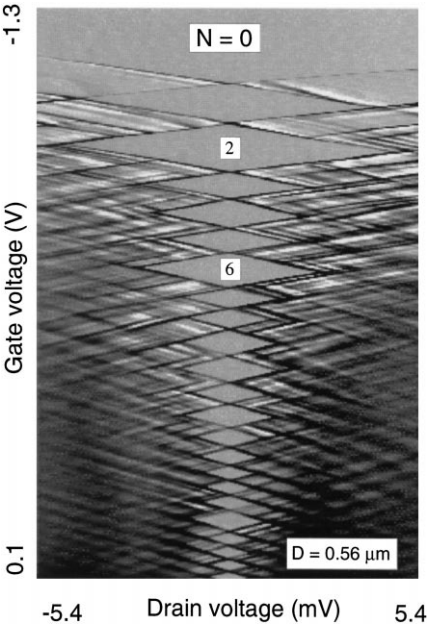

Fig. 7. Grey scale plot of $\mathrm{d}I/\mathrm{d}V_{\mathrm{sd}}$ in the V_{sd}–V_{g} plane for a $D = 0.56\,\mu$m *quantum mechanically* "strongly" coupled double dot device. Coulomb diamonds similar to those for a single dot are formed from $N = 1$ to 22 close to zero bias. The half width in eV_{sd} of a diamond shaped region is a direct measure of the change of electrochemical potential when one more electron is added to the double dot system.

line with the experimental data for $N = 1, 2$, and 3 in Fig. 2b. Note that for $N > 15$, $\mu(N+1) - \mu(N)$ is approximately half that of the single dot. This is reasonable because the double structure dot occupies roughly twice as much volume. Finally, for this *artificial molecule*, there is no evidence from Figs. 2b and 7 for the occupation of anti-symmetric states for $N \leqslant 12$, i.e. the first 12 electrons all occupy the symmetric states and are delocalized. This might look inconsistent with a single-particle picture as the symmetric and anti-symmetric states can only be distinguished in the presence of quantum mechanical coupling, and both sets of lateral states have an identical single-particle energy spectrum with a characteristic confining energy of $\hbar\omega_0$. Putting electrons consecutively into the symmetric states costs much single-particle excitation energy. For example, the complete filling of electrons in the second shell costs $4\hbar\omega_0$, which is much greater than $\Delta_{S\,AS}$. However, besides $\Delta_{S\,AS}$, there are a number of important interaction effects that determine the filling of electrons. These effects are the exchange effects within either the symmetric states or within the anti-symmetric states, are between symmetric and anti-symmetric states, screening effects, and direct Coulomb repulsion. Coulomb repulsion favours the filling of laterally delocalized electrons, i.e. p-type electrons rather than s-type electrons, so the consecutive filling of electrons in to the symmetric states is favoured. This consecutive filling is also promoted by the screening effect since it reduces the lateral confinement energy with increasing N. These three factors help to explain the experimental data for this strongly coupled dot device. The exchange effect between the symmetric and anti-symmetric states favours the filling of electrons in to the anti-symmetric states. However, this effect can be weaker than the other effects described above. Exact calculations incorporating many-body interactions are necessary for more detailed arguments. These are underway and will be discussed elsewhere.

5. Conclusions

We have studied the atomic-like properties of a single disk shaped dot and the molecular-like properties of two vertically coupled disk-shaped dots. For the single dot the addition energy spectrum for the few electron ground states at $B = 0$ T and in the presence of a magnetic field induced transitions in the ground states and these compare well to the exact calculations of many-body states in an artificial atom. For the strongly coupled double dot device the few electron ground states show properties similar to those of a single dot, indicating that the first few electrons only occupy the symmetric states and are delocalized throughout the whole system.

Acknowledgements

We thank R.J. van der Hage, M.W.S. Danoesastro, Y. Kervennic, J.E. Mooij, S.K. Nair, L.L. Sohn, and N. Uesugi for help and discussions. Part of the work is supported by the Dutch Foundation for Fundamental Research on Matter (FOM). L.P.K. is supported by the Royal Netherlands Academy of Arts and Sciences (KNAW).

References

[1] M. Reed, Scientific American 268 (1993) 118; M. Kastner, Physics Today 46 (1993) 24; R.C. Ashoori, Nature 379 (1996) 413.
[2] See for a review: Proc. Advanced Study Institute on Mesoscopic Electron Transport, Curacao, June 1996, Series E, Kluwer, Dordrecht, 1997.
[3] S. Tarucha, D.G. Austing, T. Honda, R.J. van der Hage, L.P. Kouwenhoven, Phys. Rev. Lett. 77 (1996) 3613.
[4] L.P. Kouwenhoven, T.H. Oosterkamp, M.W.S. Danoesastro, M. Eto, D.G. Austing, T. Honda, S. Tarucha, Science 278 (1997) 1788.
[5] D.G. Austing, T. Honda, S. Tarucha, Semiconductor Sci. Technol. 11 (1995) 212.
[6] S. Tarucha, D.G. Austing, T. Honda, R.J. van der Hage, L.P. Kouwenhoven, Jpn. J. Appl. Phys. 36 (1997) 3917.
[7] Y. Tokura, L.P. Kouwenhoven, D.G. Austing, S. Tarucha, Physica B 246–247 (1998) 83.
[8] This ratio of $Q/\hbar\omega_0$ is for example 1.5 for a parabolic potential with $\hbar\omega_0 = 5$ meV. It is assumed to be 1 in our previous paper (see Ref. [4]).
[9] Y. Tanaka, H. Akera, J. Phys. Soc. Japan 66 (1997) 15.
[10] See for example: J.J. Palacios, L. Martin-Moreno, G. Chiappe, E. Louis, C. Tejedor, Phys. Rev. B 50 (1994) 5760; See for more references the review by N.F. Johnson, J. Phys.: Condens. Matter 7 (1995) 965.
[11] V. Fock, Z. Phys. 47 (1928) 446; C.G. Darwin, Proc. Cambridge Phil. Soc. 27 (1930) 86.

[12] See for theory: M. Wagner, U. Merkt, A.V. Chaplik, Phys. Rev. B 45 (1992) 1951; P. Hawrylak, Phys. Rev. Lett. 71 (1993) 3374; See for experiment: B. Su, V.J. Goldman, J.E. Cunningham, Phys. Rev. B 46 (1992) 7644; R.C. Ashoori et al., Phys. Rev. Lett. 71 (1993) 613; T. Schmidt et al., Phys. Rev. B 51 (1995) 5570.

[13] D.G. Austing, T. Honda, Y. Tokura, S. Tarucha, Jpn. J. Appl. Phys. 34 (1995) 1320.

[14] D.G. Austing, T. Honda, K. Muraki, Y. Tokura, S. Tarucha, Physica B 249–251 (1998) 152.